BOUNDARY ELEMENT MODELING OF AXISYMMETRIC SUPERCAVITATING BODIES

James S. Uhlman
Abraham N. Varghese
Ivan N. Kirschner

Naval Undersea Warfare Center
Division Newport
Newport, RI 02841

31 July 1998

FROM:

PROCEEDINGS OF THE 1ST SYMPOSIUM ON MARINE APPLICATIONS OF COMPUTATIONAL FLUID DYNAMICS, 1998, MCLEAN, VA

Abstract

Slender body theory (SBT) is widely used for the numerical analysis of axisymmetric supercavitating bodies. However, due to the requirement that the slope be small, SBT cannot be used for many practical cavitator shapes such as disc and cones with large cone angles. Typically this situation would be handled by applying a nose correction to the SBT models for such cavitators. This can be avoided with a boundary element (BE) model where there is no slenderness assumption.

In this paper, boundary element modeling is applied to axisymmetric supercavitating bodies so that the cavitator shape can fully be included in the flow analysis. Mathematical formulation of the model is done with constant strength source and dipole panels, defined along the body and cavity boundary. Cavity termination is accomplished by modified Riabouchinsky wall. The full nonlinear free-boundary problem is solved. Different cavitator geometries at a variety of cavitation numbers are analyzed in this paper for cavity shape, surface pressure distribution, and base drag. Comparisons with experimental and analytical models are also done.

Nomenclature

ρ	Fluid density
d	Cavitator diameter
U_∞	Vehicle speed
Φ	Total velocity potential
ϕ	Disturbance velocity potential
$\mathbf{U}$	Fluid total velocity
$\mathbf{u}$	Fluid disturbance velocity
p	Fluid pressure

Introduction

Interest in high-speed undersea vehicles has recently increased. In order to achieve the speeds of interest it becomes necessary to investigate supercavitating and superventilated flows. It is believed that, with proper design, these flows can be employed to attain vehicle drags which will allow these vehicles to achieve the desired speeds.

Early work on cavitating flows was done by Efros (1946), who employed conformal mapping techniques to examine supercavitating flows. Tulin (1964) introduced the use of perturbation methods to the field in the examination of two dimensional flows, while Chou (1974) extended that work to axisymmetric supercavitating flows using slender body theory. Early numerical approaches include that of Brennan (1969), who employed a mapping technique. Nonlinear boundary element models were developed by Uhlman (1987, 1989) and Kinnas and Fine (1990, 1993) among others.

This work represents an application of the methods of Uhlman (1987, 1989) and Kinnas and Fine (1990, 1993) to supercavitating bodies. These methods are also being extended to include ventilation and blockage effects. Work is continuing on the extension of these methods to improved cavity termination models and three dimensional flows.

Mathematical Formulation

Defining the disturbance potential by

$$\Phi = U_\infty(x + \phi) \tag{1}$$

we find that the integral equation for the disturbance potential is

$$2\pi\phi = -\int_C \left\{\frac{\partial\phi}{\partial n} G - \phi \frac{\partial G}{\partial n}\right\} ds \tag{2}$$

where G is the axisymmetric Green's function (see Appendix A), C denotes the total flow boundary contour including the cavitator or body boundary, the cavity wall and the boundary of the cavity terminator and the normal to the boundary is pointing into the fluid. Bernoulli's equation yields

$$p_\infty + \frac{1}{2}\rho U_\infty^2 = p_c + \frac{1}{2}\rho q_c^2 \tag{3}$$

or

$$\left(\frac{q}{U_\infty}\right)^2 = 1 + \sigma \tag{4}$$

where σ is the cavitation number defined as

$$\sigma = \frac{(p_\infty - p_c)}{\frac{1}{2}\rho U_\infty^2} \tag{5}$$

The result in equation (4) may then be employed to obtain the dynamic boundary condition on the cavity boundary given by

$$s_x + \frac{\partial \phi}{\partial s} = \sqrt{1+\sigma} \tag{6}$$

Finally, to complete the formulation we require a closure condition which may be written as

$$\int_{C_B + C_C} \frac{\partial \phi}{\partial n} \frac{dS}{ds}\, ds = 0 \tag{7}$$

where C_B denotes the union of the body and cavity terminator boundaries and C_C denotes the cavity boundary.

Thus, on the body and cavity terminator contours, C_B, the integral equation is given by

$$2\pi\phi - \int_{C_B} \phi \frac{\partial G}{\partial n}\, ds + \int_{C_C} \frac{\partial \phi}{\partial n} G\, ds = - \int_{C_B} \frac{\partial \phi}{\partial n} G\, ds + \int_{C_C} \phi \frac{\partial G}{\partial n}\, ds \tag{8}$$

and on the cavity surface, C_C, the integral equation is given by

$$- \int_{C_B} \phi \frac{\partial G}{\partial n}\, ds + \int_{C_C} \frac{\partial \phi}{\partial n} G\, ds = - 2\pi\phi - \int_{C_B} \frac{\partial \phi}{\partial n} G\, ds + \int_{C_C} \phi \frac{\partial G}{\partial n}\, ds \tag{9}$$

with the closure condition

$$\int_{C_C} \frac{\partial \phi}{\partial n} \frac{dS}{ds}\, ds = - \int_{C_B} \frac{\partial \phi}{\partial n} \frac{dS}{ds}\, ds \tag{10}$$

Note, however, that equation (6) implies that, on the cavity boundary,

$$\phi = \phi_0 + \sqrt{1+\sigma}\,(s - s_0) - (x - x_0) \tag{11}$$

The required equations then become

$$2\pi\phi - \int_{C_B} \phi \frac{\partial G}{\partial n} ds + \int_{C_C} \frac{\partial \phi}{\partial n} G\, ds - \sqrt{1+\sigma} \int_{C_C} (s - s_0) \frac{\partial G}{\partial n} ds$$
$$= - \int_{C_B} \frac{\partial \phi}{\partial n} G\, ds + \phi_0 \int_{C_C} \frac{\partial G}{\partial n} ds - \int_{C_C} (x - x_0) \frac{\partial G}{\partial n} ds \qquad (12)$$

on the body and cavity terminator boundaries, and

$$- \int_{C_B} \phi \frac{\partial G}{\partial n} ds + \int_{C_C} \frac{\partial \phi}{\partial n} G\, ds - \sqrt{1+\sigma} \left[- 2\pi (s - s_0) + \int_{C_C} (s - s_0) \frac{\partial G}{\partial n} ds \right]$$
$$= - 2\pi \left[\phi_0 - (x - x_0) \right] - \int_{C_B} \frac{\partial \phi}{\partial n} G\, ds + \phi_0 \int_{C_C} \frac{\partial G}{\partial n} ds - \int_{C_C} (x - x_0) \frac{\partial G}{\partial n} ds \qquad (13)$$

on the cavity boundary.

These equations represent a mixed boundary value problem. The unknowns over the wetted portions of the flow boundary are the values of the disturbance potential, while over the cavity boundary the unknowns are the values of the normal derivative of the potential.

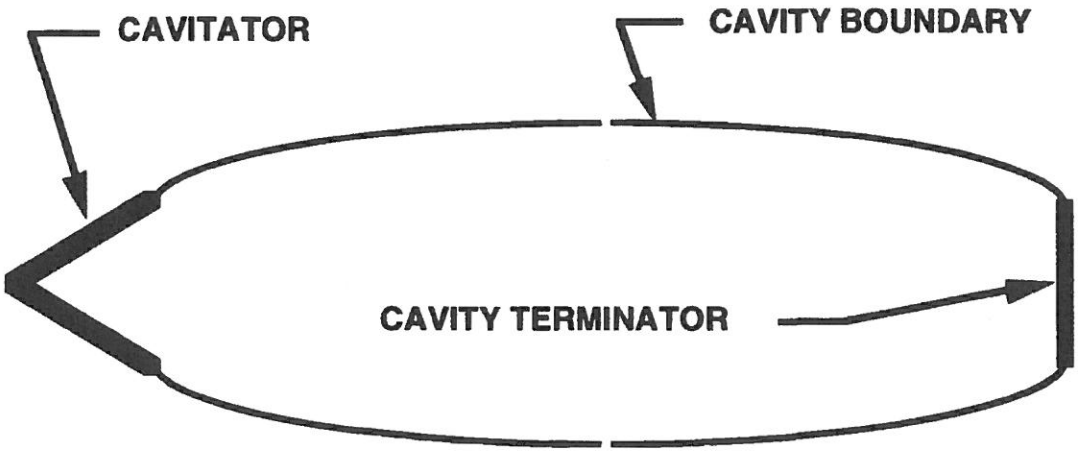

Figure 1 An illustration of the cavitator, cavity and cavity terminator.

Cavity Termination Models

The modeling of the closure of the cavity is, perhaps, the most controversial aspect of the numerical simulation of cavitating flows. Certainly, for sufficiently high Froude number, the correct laminar model for axisymmetric flows is the reentrant jet model (see figure 2).

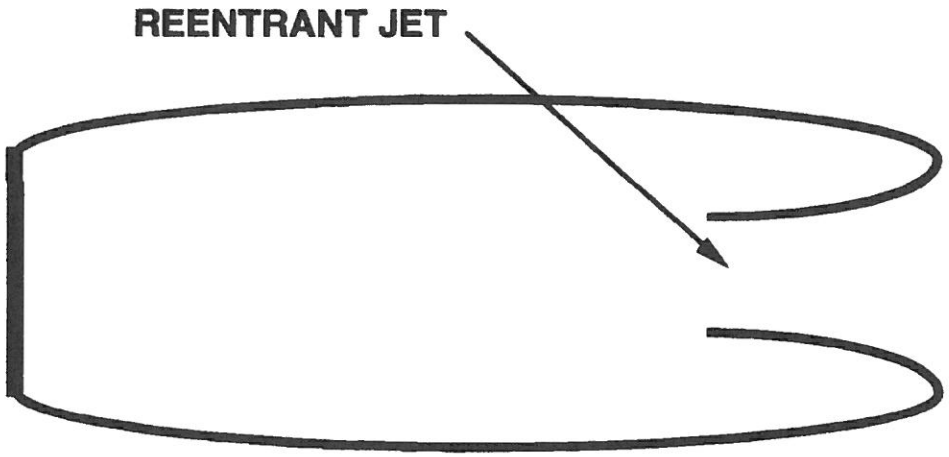

Figure 2 An illustration of a reentrant jet cavity termination model.

However, in the interest of expediency, the cavity termination model we have employed here is the so-called, "modified Riabouchinsky model," (see Uhlman 1987, 1989 and figure 1). It may be argued that the salient feature which both models possess is a stagnation point in the flow in the vicinity of the end of the cavity. In addition, due to the nature of elliptic flows it can certainly be argued that, for sufficiently long cavities, the nature of the cavity termination should have only a small effect on the behavior of the cavity near the cavitator. Further examination of the effect of cavity termination models on cavitation parameters will have to await the development of a reentrant jet model (see Uhlman 1999). Finally, it should be noted that for low Froude number flows, there also exists another steady cavity termination model referred to as the twin vortex model.

Solution Procedure

Following the work of Uhlman (1987, 1989) the procedure for the solution of the nonlinear problem consists of:

i) selecting a cavity length,
ii) initializing the cavity shape
iii) formulating the mixed boundary value problem for the existing cavity shape, wherein the kinematic boundary condition of no-flux is enforced on the wetted portions of the boundary and the dynamic boundary condition of constant pressure is enforced on the boundary of the cavity,

iv) solving the mixed boundary value problem on the existing cavity shape, yielding the value of the cavitation number and the values over the boundary of the disturbance potential and its normal derivative,

v) updating the cavity shape by using the kinematic boundary condition over the cavity,

v) iterating to convergence.

This procedure or algorithm is presented the form of a flow chart in figure 3.

Cavity Shape Update

In order to update the cavity shape approximation the kinematic boundary condition is employed. The kinematic boundary condition on a given panel is written as

$$\mathbf{n} \cdot \mathbf{u} = 0 \tag{14}$$

where it is assumed that the velocity is known from the solution of the integral equations and the normal is written as

$$n_x = -\frac{\Delta y + \delta y}{\Delta s}$$
$$n_y = \frac{\Delta x + \delta x}{\Delta s} \tag{15}$$

where

$$\Delta s^2 = \Delta x^2 + \Delta y^2 \tag{16}$$

and the quantities δx and δy are to be determined. Equation (14) then becomes

$$v\,\delta x - u\,\delta y = u\,\Delta y - v\,\Delta x \tag{17}$$

and another equation must be introduced to allow us to solve for δx and δy. The simplest approach is to assume that δx is zero, this then yields the result that

$$\delta y = \frac{v\,\Delta x - u\,\Delta y}{u} \tag{18}$$

This displacement is then applied to the panel from which it was derived and all downstream panels.

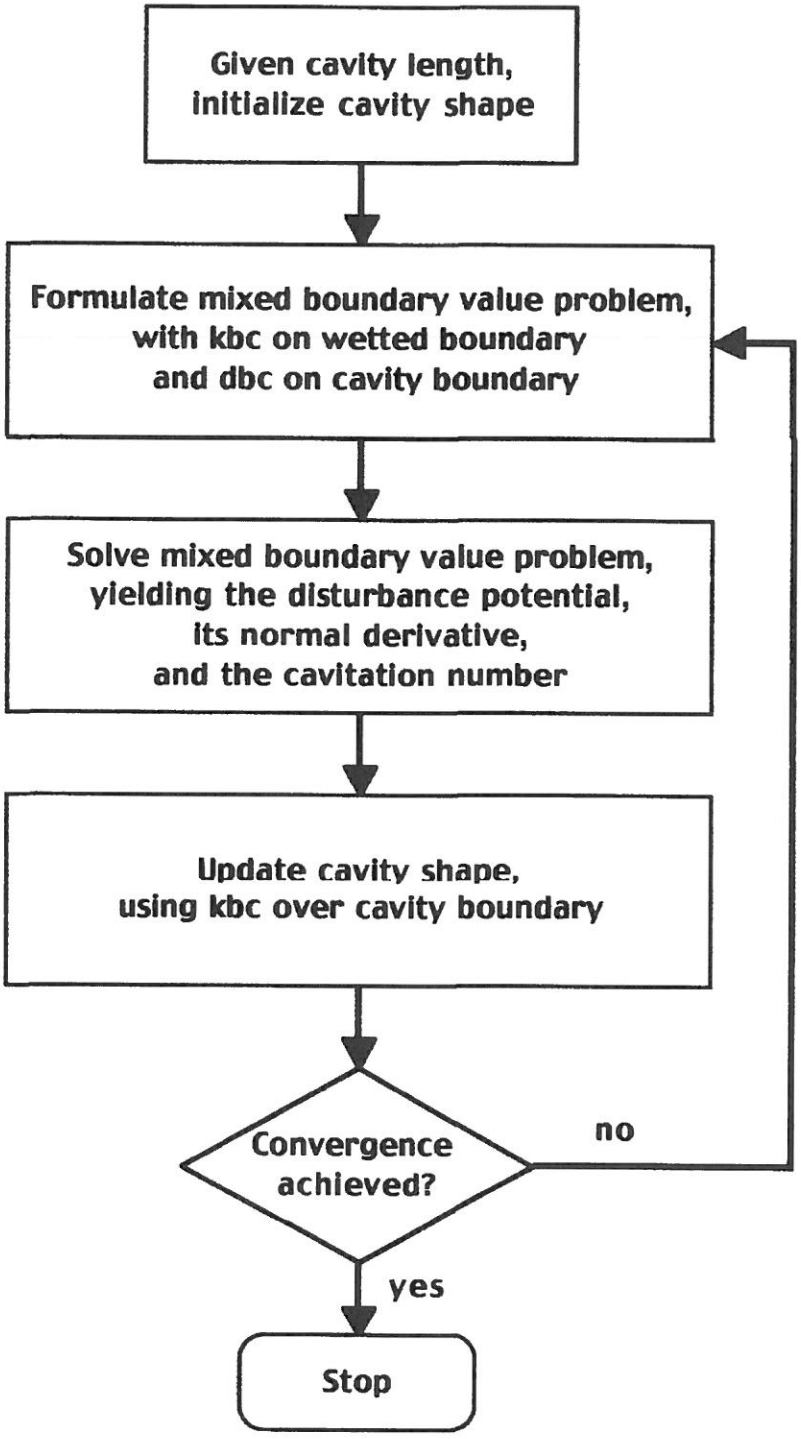

Figure 3 A flow chart of the solution algorithm employed.

Alternatively, one might require that

$$(\Delta x + \delta x)^2 + (\Delta y + \delta y)^2 = \Delta s^2 \tag{19}$$

which, when linearized yields

$$\Delta x\, \delta x + \Delta y\, \delta y = 0 \tag{20}$$

From these equations we then find that

$$\begin{aligned} \delta x &= \Delta y \left(\frac{u\,\Delta y - v\,\Delta x}{u\,\Delta x + v\,\Delta y} \right) \\ \delta y &= \Delta x \left(\frac{v\,\Delta x - u\,\Delta y}{u\,\Delta x + v\,\Delta y} \right) \end{aligned} \tag{21}$$

Computation of Forces

Forces are computed from integration of the pressures over the relevant boundaries. Specifically, the drag on the cavitator is computed by integrating the fluid pressure over the wetted portion of the cavitator and subtracting the force due to the constant cavity pressure acting over the aft face of the cavitator. The pressures in the fluid are computed from the velocities via Bernoulli's theorem.

The velocities are computed from the values of the potential and its normal derivative over the boundary. This is accomplished by taking the derivatives of the disturbance potential and the coordinates with respect to arclength along the flow boundary to obtain the quantities

$$s_x,\ s_y,\ \text{and}\ \frac{\partial \phi}{\partial s}$$

at the control points of the panels. Since the normal derivative and the components of the normal are already known, we may then form the equations

$$\begin{aligned} s_x\, u + s_y\, v &= \frac{\partial \phi}{\partial s} \\ n_x\, u + n_y\, v &= \frac{\partial \phi}{\partial n} \end{aligned} \tag{22}$$

where u and v represent the components of the disturbance velocity. These equations may then be solved for u and v and their values may be used to compute the pressure.

Ventilation Case

Define the disturbance velocity potential for the external flow, ϕ^+, by

$$\Phi^+ = U_\infty(x + \phi^+) \tag{23}$$

Then the integral equation for the external disturbance potential is

$$2\pi\phi^+ = -\int_C \left\{\frac{\partial\phi^+}{\partial n^+} G - \phi^+ \frac{\partial G}{\partial n^+}\right\} ds \tag{24}$$

where G is the axisymmetric Green's function.

Assuming irrotational flow of an incompressible fluid on the interior of the cavity as well, we may define a velocity potential for the internal cavity flow, ϕ^-, by

$$\Phi^- = U_\infty\phi^- \tag{25}$$

The kinematic boundary condition on the body/cavity boundary is then given by

$$\begin{aligned} \frac{\partial\phi^+}{\partial n^+} &= -n_x \\ \frac{\partial\phi^-}{\partial n^-} &= 0 \end{aligned} \tag{26}$$

In the external flow Bernoulli's equation yields

$$p_\infty + \frac{1}{2}\rho^+U_\infty^2 = p^+ + \frac{1}{2}\rho^+(q^+)^2 \tag{27}$$

or

$$\left(\frac{q^+}{U_\infty}\right)^2 = 1 + \left(\frac{p_\infty - p^+}{\frac{1}{2}\rho^+U_\infty^2}\right) \tag{28}$$

In the internal flow, Bernoulli's equation yields

$$p^- + \frac{1}{2}\rho^-(q^-)^2 = H \tag{29}$$

Equality of pressure across the cavity interface then requires that

$$\left(\frac{q^+}{U_\infty}\right)^2 = 1 + \left(\frac{p_\infty - H}{\frac{1}{2}\rho^+U_\infty^2}\right) + \left(\frac{\rho^-}{\rho^+}\right)\left(\frac{q^-}{U_\infty}\right)^2 \tag{30}$$

Hence, if we define

$$\sigma = \frac{(p_\infty - H)}{\frac{1}{2}\rho^+ U_\infty^2} \tag{31}$$

then the dynamic boundary condition on the cavity exterior becomes

$$\left(\frac{q^+}{U_\infty}\right)^2 = \left[(1+\sigma) + \left(\frac{\rho^-}{\rho^+}\right)\left(\frac{q^-}{U_\infty}\right)^2\right]^{\frac{1}{2}} \tag{32}$$

which may be written as

$$s_x + \frac{\partial \phi^+}{\partial n^+} = \sqrt{(1+\sigma)}\left[1 + \frac{1}{(1+\sigma)}\left(\frac{\rho^-}{\rho^+}\right)\left(\frac{q^-}{U_\infty}\right)^2\right]^{\frac{1}{2}} \tag{33}$$

which may be integrated to yield

$$\phi^+ = \phi_0^+ - (x - x_0) + \sqrt{(1+\sigma)}\, F(s) \tag{34}$$

where

$$F(s) = \int_{s_0}^{s}\left[1 + \frac{1}{(1+\sigma)}\left(\frac{\rho^-}{\rho^+}\right)\left(\frac{q^-}{U_\infty}\right)^2\right]^{\frac{1}{2}} ds \tag{35}$$

Thus, on the body and cavity terminator contours, C_B, the integral equation for the external flow is given by

$$\begin{aligned} 2\pi\phi - \int_{C_B} \phi \frac{\partial G}{\partial n}\, ds + \int_{C_C} \frac{\partial \phi}{\partial n} G\, ds - \sqrt{1+\sigma}\int_{C_C} F(s)\frac{\partial G}{\partial n}\, ds \\ = -\int_{C_B} \frac{\partial \phi}{\partial n} G\, ds + \phi_0 \int_{C_C} \frac{\partial G}{\partial n}\, ds - \int_{C_C} (x - x_0)\frac{\partial G}{\partial n}\, ds \end{aligned} \tag{36}$$

and on the cavity surface, C_C, the integral equation is given by

$$- \int_{C_B} \phi \frac{\partial G}{\partial n} ds + \int_{C_C} \frac{\partial \phi}{\partial n} G \, ds - \sqrt{1+\sigma} \left[- 2\pi F(s) + \int_{C_C} F(s) \frac{\partial G}{\partial n} ds \right]$$

$$= - 2\pi \left[\phi_0 - (x - x_0) \right] - \int_{C_B} \frac{\partial \phi}{\partial n} G \, ds + \phi_0 \int_{C_C} \frac{\partial G}{\partial n} ds - \int_{C_C} (x - x_0) \frac{\partial G}{\partial n} ds \tag{37}$$

with the closure condition

$$\int_{C_C} \frac{\partial \phi}{\partial n} \frac{dS}{ds} ds = - \int_{C_B} \frac{\partial \phi}{\partial n} \frac{dS}{ds} ds \tag{38}$$

The flow on the interior of the cavity is computed as a straight potential flow with kinematic boundary conditions applied. It is the goal of the present effort to demonstrate that this approach to solving the coupled problem does, in fact, converge. The current approach has been to solve the interior flow using a finite element method. The finite element method has been employed with the idea that it could later be extended to handle more complicated flows without impacting the coupling between the internal and external flows.

It should be noted that this ventilation model is incomplete. What remains to be developed is model for the loss of ventilation gas from the cavity. From the experimental results of May (1975) there appear to be at least three regimes. In the first regime the gas loss seems to be due to entrainment in the reentrant jet and is reasonably steady. The second regime involves gas loss through the shedding of toriodal bubbles from the back of the cavity and is highly unsteady. In the third regime the cavity has entered the so-called twin vortex mode and the gas loss is again steady. In the first regime the dependence of the effective cavitation number on the gas flow rate is quite strong. In the third regime the gas is passing out the twin trailing vortices and there is only a weak dependence of the effective cavitation number on gas flow rate. the second regime represents a transition between the first and third. In our present model we have assumed that the gas which flows into the cavity, flows out through the cavity termination wall at the same net flow rate. This results in a very weak dependence of the cavitation number on gas flow rate.

Results

The first set of results to be presented will examine natural cavitation past axisymmetric cavitators of differing shapes. Figures 4 and 5 present the cavity shapes for disk and cone cavitators at identical cavitation numbers. The length scales are dimensionless with respect to the base diameter of the cavitator. It is readily seen that, for a given cavitation number, the disk cavitator leads to longer cavities and cavities with greater maximum diameters.

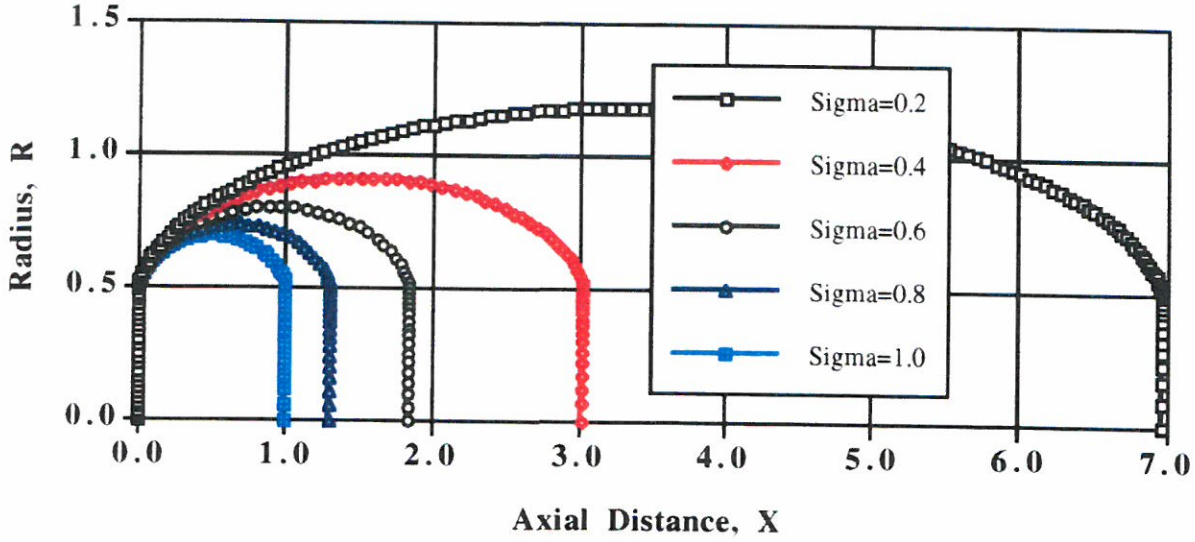

Figure 4 Cavity shapes for a disk cavitator at a variety of cavitation numbers.

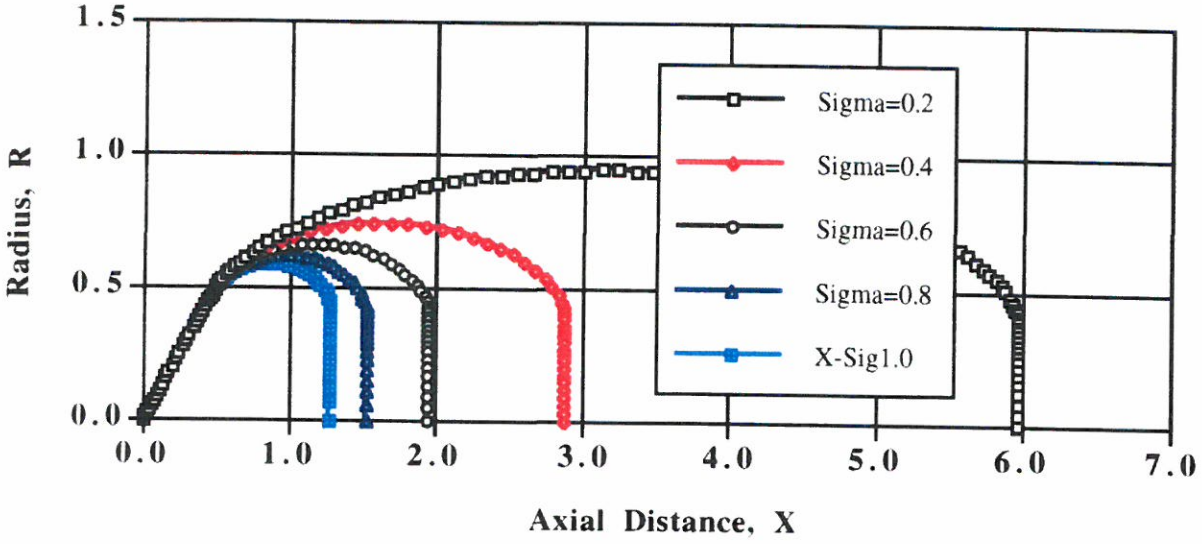

Figure 5 Cavity shapes for a cone cavitator at a variety of cavitation numbers.

Figures 6 through 8 present the dependence on cavitation number of the dimensionless cavity length, the dimensionless maximum cavity diameter and the drag coefficient respectively. The results for both the disk and the cone cavitators are presented. Again, it is seen that the disk yields longer and wider cavities at a given cavitation number. In addition, it is seen that the drag associated with the cavitation is substantially higher for the disk cavitator than for the cone.

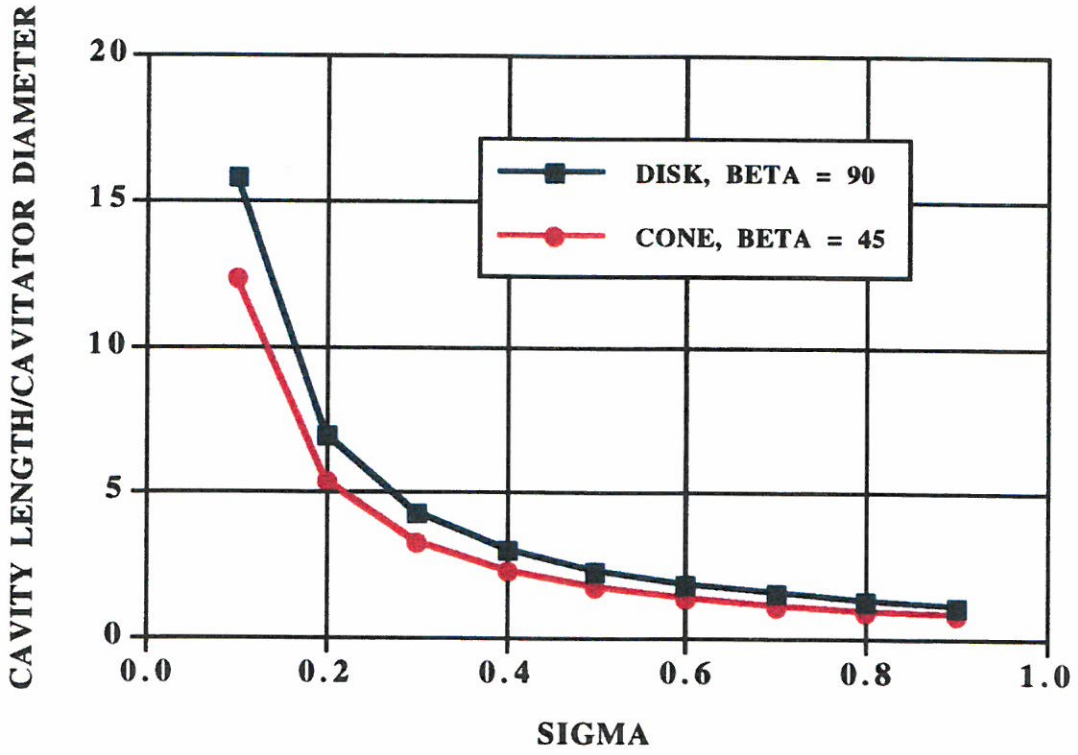

Figure 6 Dimensionless cavity length versus cavitation number for disk and cone cavitators.

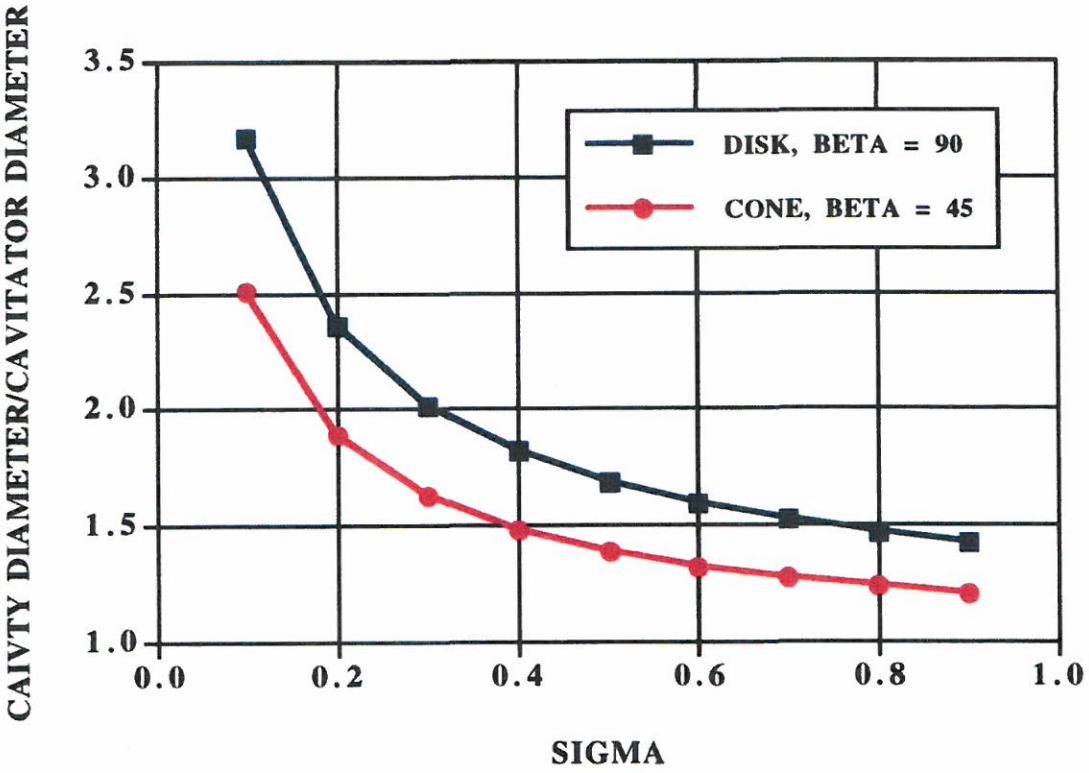

Figure 7 Dimensionless cavity diameter versus cavitation number for disk and cone cavitators.

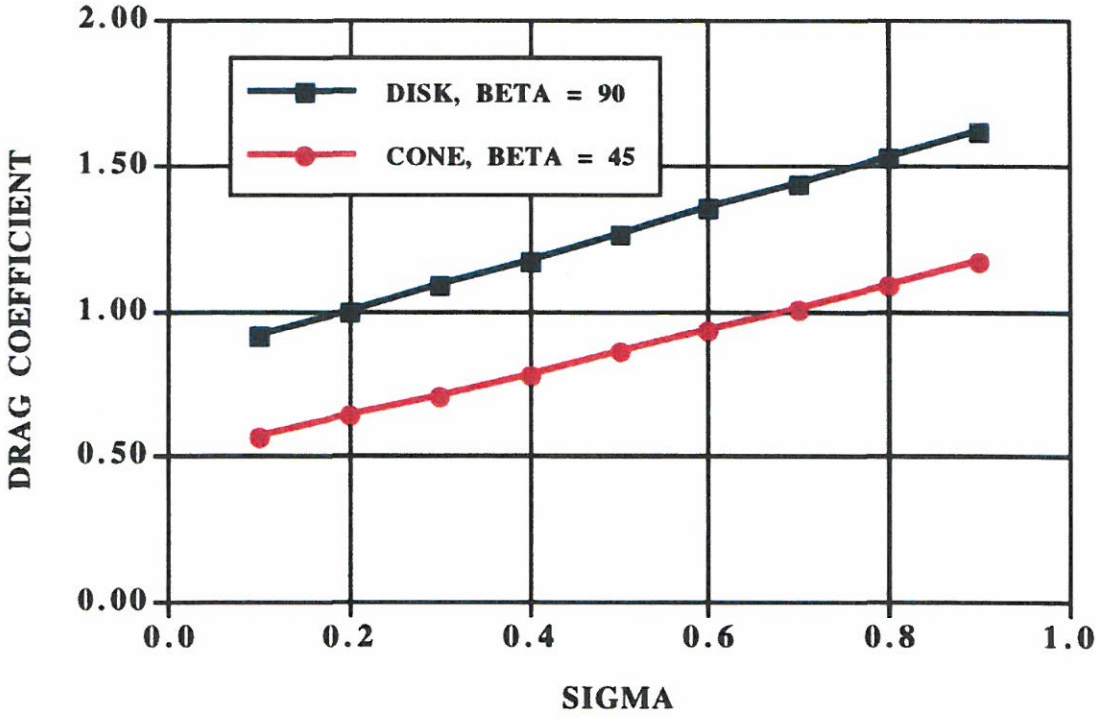

Figure 8 Drag coefficient versus cavitation number for disk and cone cavitators.

Figures 9, 10 and 11 present comparisons of the predictions of the present method with experimental results found in May (1975). Figure 9 presents the dependence of the drag coefficient of a disk with the cavitation number, while figure 10 presents the same data for a cone. The agreement in both cases is good, with the predictions falling within the experimental scatter. If anything, the predictions appear to be slightly on the high side. This is particularly curious in the case of the cone since viscous drag contributions have not been taken into account.

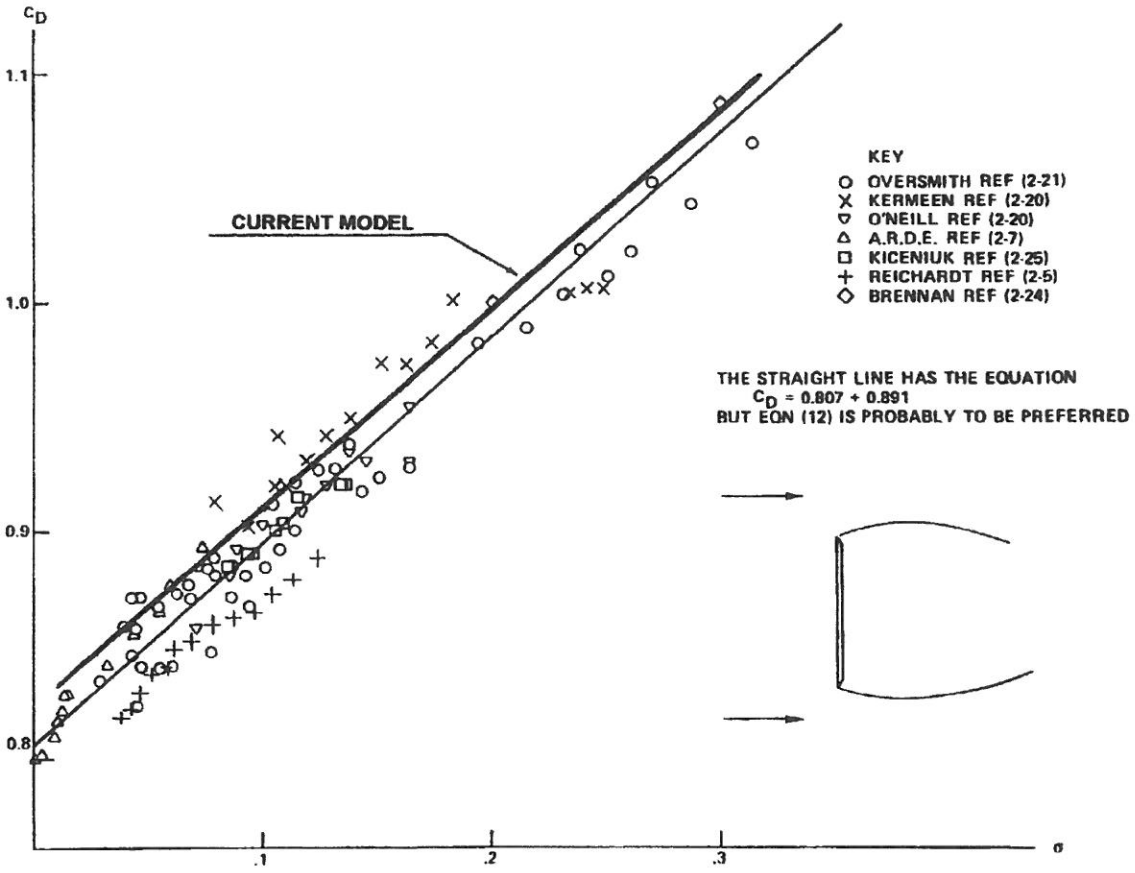

Figure 9 Drag coefficient versus cavitation number for a disk (from May 1975).

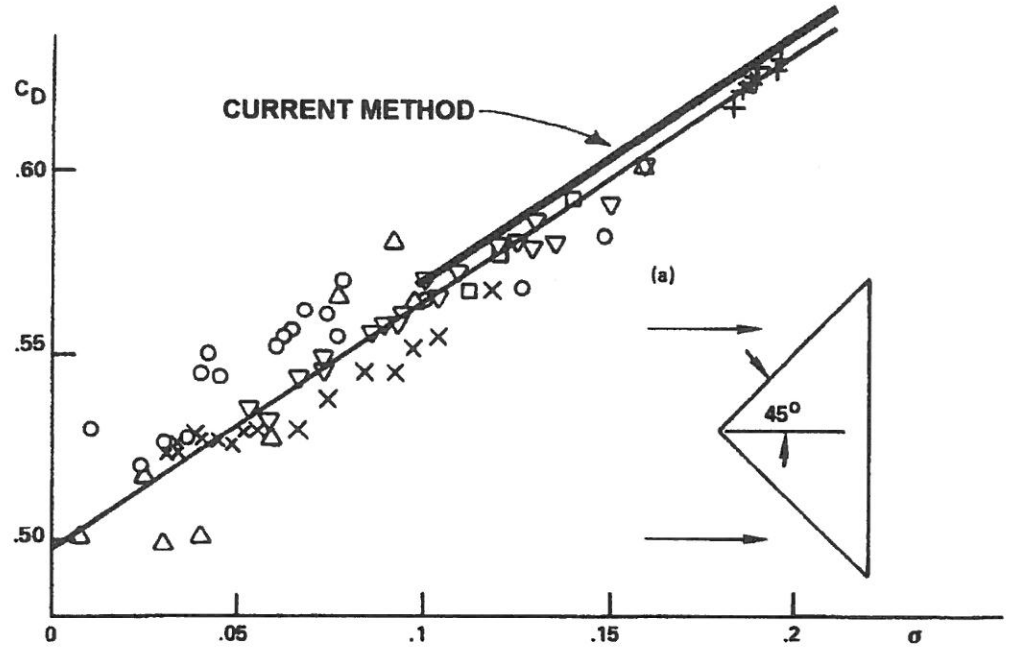

Figure 10 Drag coefficient versus cavitation number for a cone (from May 1975).

Figure 11 presents the dependence of the cavity length on cavitation number for a disk. In this case the length has been normalized with respect to the inverse square root of the drag coefficient following the work of Garabedian (1956). Again, the agreement of the predictions with the data is good.

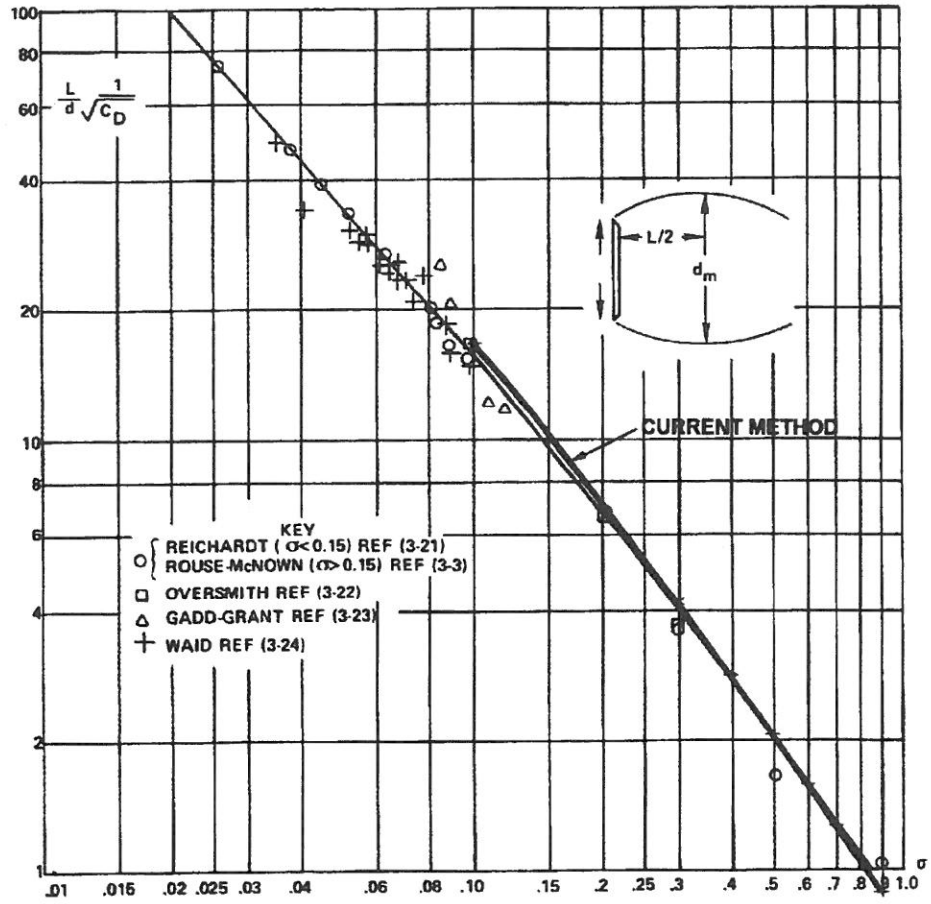

Figure 11 Normalized cavity length versus cavitation number for a disk (from May 1975).

Figures 12 and 13 present the predicted and experimental dependence of the drag coefficient, for sigma-shaped cavitators, on axial cavitator length for four different cone half-angles. The results in figure 13 are for zero cavitation number, while those in figure 12 have been scaled to zero cavitation number based on the assumption that

$$C_D = C_{D_0}(1 + \sigma) \tag{39}$$

It is readily seen that, although the trend is correct, the computations overpredict the drag coefficient. It is suspected that this is due to the existence of recirculation regions in the reetrant corners of the cavitator in real fluids, as such effects would tend to lessen the pressures experienced by the cavitator in those regions. The potential flow calculations, on the other hand, will predict stagnation point pressures at all reentrant corners, leading to higher drags.

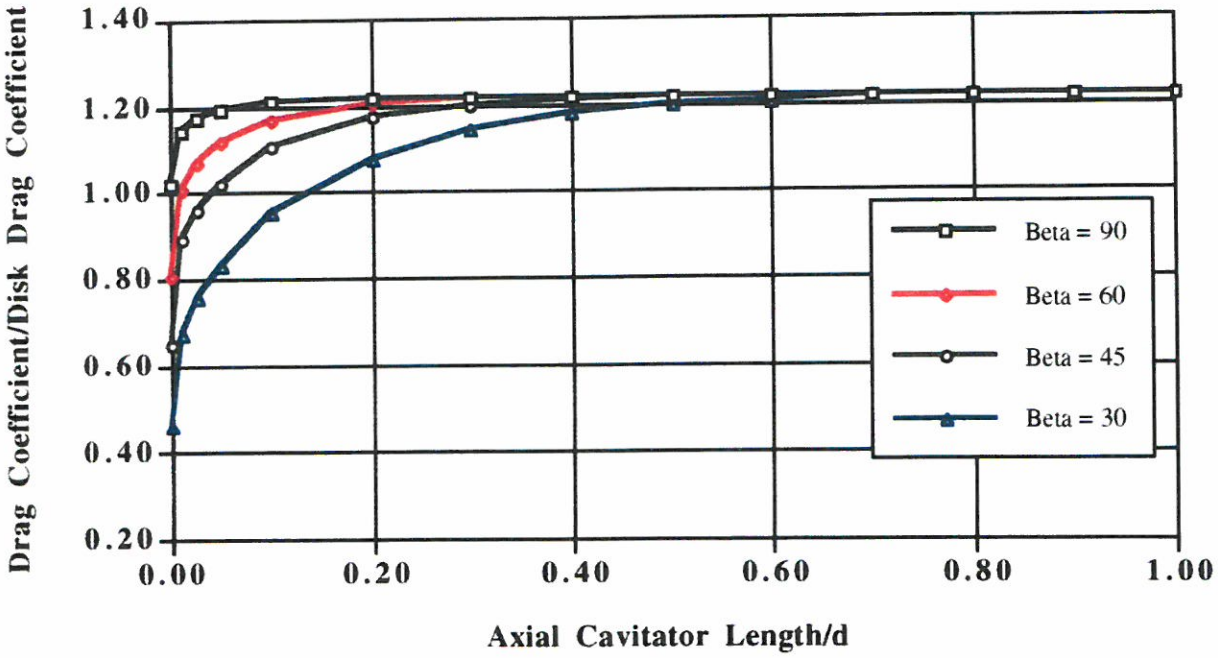

Figure 12 Drag coefficient versus cavitator length for sigma shaped cavitators.

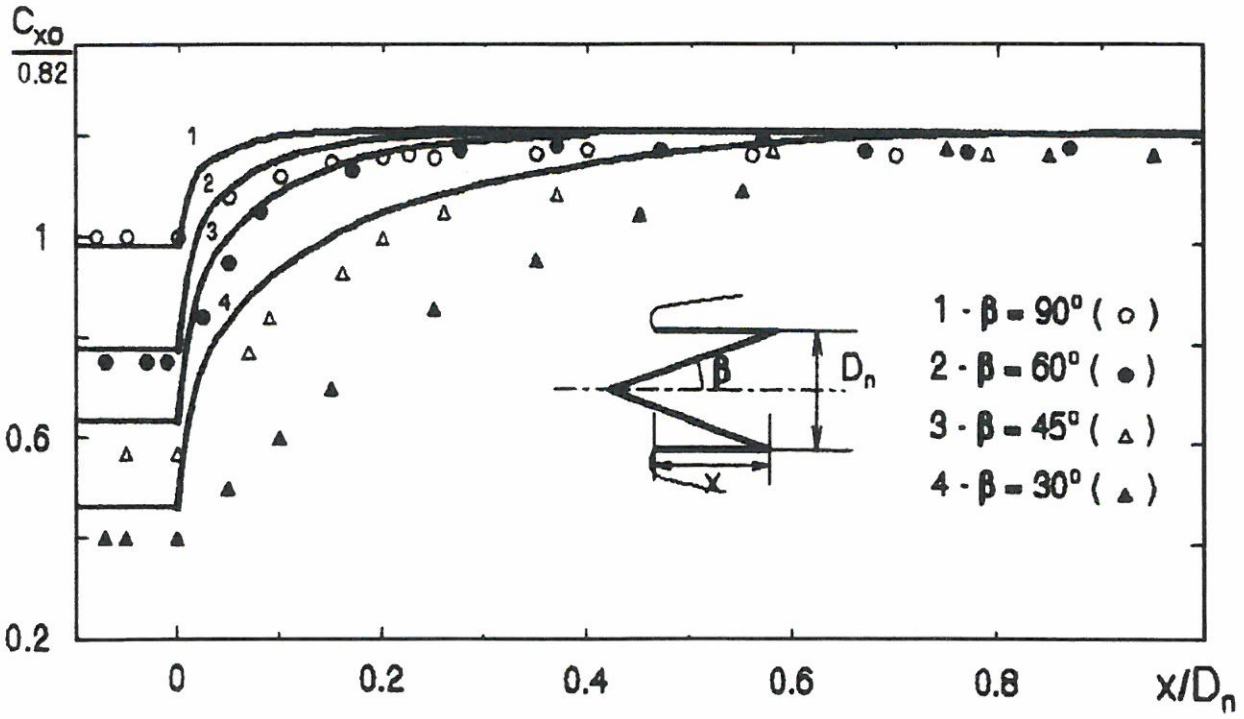

Figure 13 Drag coefficient versus cavitator length for sigma shaped cavitators (from Savchenko et al. 1997).

Figure 14 shows a comparison of the cavity shapes for a sigma-shaped cavitator and a cone cavitator of the same half-angle. The cavity shapes for the cone are presented at the same cavitation number as the sigma-shaped cavitator and the same cavity length. As might be expected, for a given cavitation number the sigma cavitator produces a cavity which is both longer and larger in diameter. Even for a cavity of the same length, the sigma cavitator produces a cavity of significantly greater diameter. The penalty for this volume increase is a large increase in the drag experienced by the cavitator.

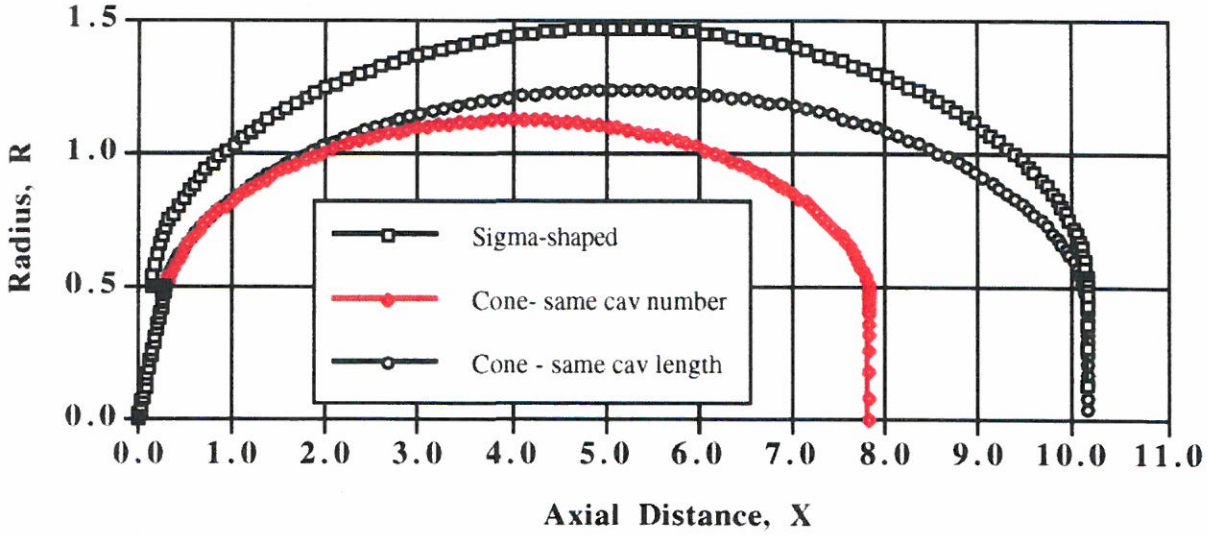

Figure 14 A comparison of the cavity produced by a sigma-shaped cavitator with that of a cone at the same cavitation number and at the same cavity length (sigma-shaped cavitator $\sigma = 0.169$, $C_D = 1.136$; cone cavitator $\sigma = 0.169$, $C_D = 0.765$ and 0.135, $C_D = 0.740$).

Figures 15 and 16 present preliminary results for the ventilated cavity model. Due to the nonphysical model employed for the gas loss we have had to specify very large gas flow rates to see any effect. Figure 15 compares the shape of the cavity for a ventilated and unventilated case at the same cavity length. It is seen that the ventilation tends to reduce the diameter of the cavity while raising/lowering the cavitation number. Figure 16 presents the pressure distribution inside the cavity as computed by a finite element method showing that the pressure does vary within the cavity.

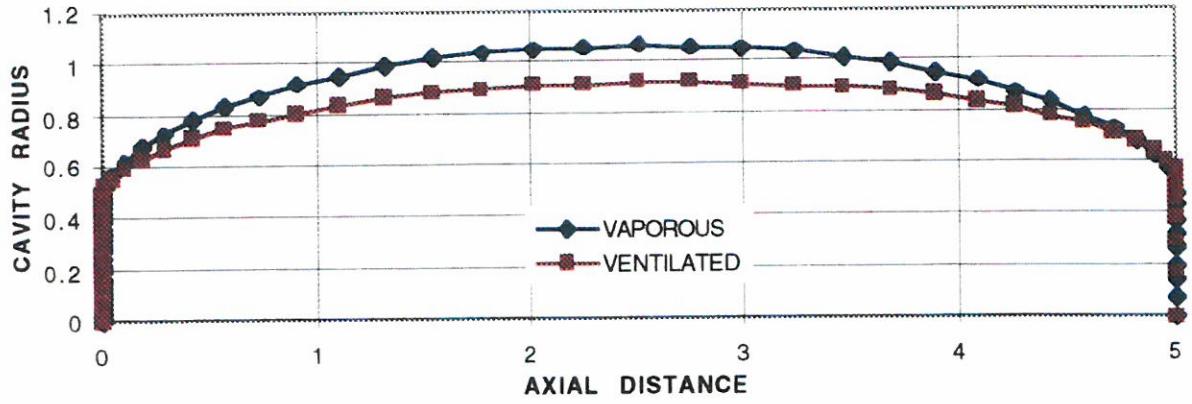

Figure 15 Cavity shape determined for ventilated flow (unventilated $\sigma = 0.266$, ventilated $\sigma = 0.090$, $C_Q = 30$)

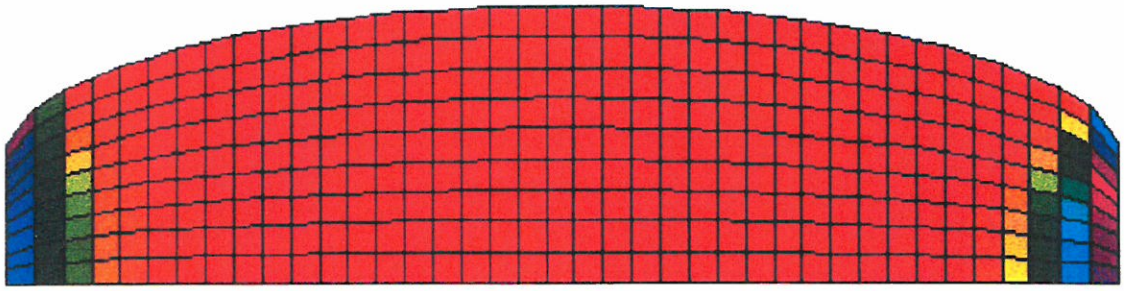

Figure 16 Pressure contours inside cavity with ventilation.

Conclusions

The results presented show that the basic calculation method for unventilated axisymmetric cavitation is well in hand. We are able to compute fully nonlinear cavity flows readily, with well defined cavity boundaries and good agreement for the drag coefficients. Work is continuing on the development of improved cavity termination models and the extension of these methods to three-dimensional cavities with transverse gravity fields.

The situation is not as well developed for ventilated problems. It appears that the ventilated problem may be viewed as consisting of three subproblems, how to get the gas into the cavity, how to model the behavior of the gas while it is in the cavity and how to get the gas back out of the cavity. The first subproblem is fairly simple and has been solved here by merely introducing the ventilation gas at the back side of the cavitator. The second subproblem is somewhat more involved, but has been solved in the potential flow limit by matching pressures across the cavity boundary as described earlier. The third subproblem is more difficult. Work is continuing on the development of physical models for the gas loss. It is hoped that these developments will be able to be reported soon.

Acknowledgments

This work was supported, in part, by the Office of Naval Research (ONR) under the sponsorship of Mr. J. Fein under program element number 61153N. This work was also supported, in part, by the In-House Laboratory Independent Research (ILIR) program administered by Dr. S. Dickinson, program element number 61152N.

References

Abramowitz, M. and I.A. Stegun, (1972), Handbook of Mathematical Functions, National Bureau of Standards, Applied Mathematics Series 55.

Brennan, C., (1969), A Numerical Solution of Axisymmetric Cavity Flows, J. Fluid, Mechanics, Vol. 37, Part 4, pp. 671-688.

Chou, Y.S. (1974), Axisymmetric Cavity Flows Past Slender Bodies of Revolution, Journal of Hydronautics, Vol. 8, No. 1.

Efros, D.A., (1946), Hydrodynamic Theory of Two-Dimensional Flow with Cavitation, Dokl. Akad. Nauk. SSSR, Vol. 51, pp. 267-270.

Garabedian, P.R., (1956), Calculation of Axially Symmetric Cavities and Jets, Pac. J. Math., Vol. 6, pp. 611-684

Gradshteyn, I.S. and I.W. Ryzhik, (1965), Table of Integrals, Series and Products, Academic Press, New York, NY

Kinnas, S.A., and N.E. Fine, (1993), A Numerical Nonlinear Analysis of the Flow Around Two- and Three-Dimensional Partially Cavitating Hydrofoils, Journal of Fluid Mechanics, Vol. 254.

Kinnas, S.A., and N.E. Fine, (1990), Non-Linear Analysis of the Flow Around Partially and Super-Cavitating Hydrofoils by a Potential Based Panel Method, Proceedings of the IABEM-90 Symposium, International Association for Boundary Element Methods, Rome, Italy.

Kirschner, I.N., J.S. Uhlman, Jr., A.N. Varghese, and I.M. Kuria, (1995), Supercavitating Projectiles in Axisymmetric Subsonic Liquid Flows, Proceedings of the ASME & JSME Fluids Engineering Annual Conference & Exhibition, Cavitation and Multiphase Flow Forum, FED 210, J. Katz and Y. Matsumoto, editors, Hilton Head Island, SC.

Kuria, I.M., I.N. Kirschner, A.N. Varghese, and J.S. Uhlman, (1997), Compressible Cavity Flows Past Slender Non-Lifting Bodies of Revolution, Proceedings of the ASME & JSME Fluids Engineering Annual Conference & Exhibition, Cavitation and Multiphase Flow Forum, FEDSM97-3262, Vancouver, BC.

May, A., (1975), Water Entry and the Cavity-Running Behavior of Missiles, SEAHAC Technical Report 75-2, Naval Surface Weapons Center, White Oak Laboratory, Silver Spring, MD.

Savchenko, Y.N., V.N. Semenenko, Y.I. Naumova, A.N. Varghese, J.S. Uhlman, and I.N. Kirschner, (1997), Hydrodynamic Characteristics of Polygonal Contours in Supercavitating Flow, Proceedings of the Third International Symposium on Performance Enhancement for Marine Applications , Newport, RI, 1997.

Tulin, M. P., (1964), Supercavitating flows - small perturbation theory, J. Ship Research, Vol. 7, No. 3, pp. 17-37.

Uhlman, J.S., (1987), The Surface Singularity Method Applied to Partially Cavitating Hydrofoils, Journal of Ship Research, Vol. 31, No. 2, pp. 107-124.

Uhlman, J.S., (1989), The Surface Singularity or Boundary Integral Method Applied to Supercavitating Hydrofoils, Journal of Ship Research, Vol. 33, No. 1, pp. 16-20.

Uhlman, J.S., (1998), A Derivation of Axisymmetric Potential Flow Influence Functions for Use in Boundary Integral Methods, (in preparation).

Uhlman, J.S., (1998), A Reentrant Jet Model for Axisymmetric Supercavitation, (in preparation).

Varghese, A.N., J.S. Uhlman, and I.N. Kirschner, (1997), Axisymmetric Slender-Body Analysis of Supercavitating High-Speed Bodies in Subsonic Flow, Proceedings of the Third International Symposium on Performance Enhancement for Marine Applications , Newport, RI, 1997.

Wu, T.Y., (1968), Inviscid cavity and wake flows, Basic Developments in Fluid Dynamics, No. 2, pp. 1-116.

Appendix A

Derivation of Green's Third Identity for Axisymmetric Problems

Green's third identity in three dimensions is given by

$$\beta\phi = \iint_S \left\{ \phi \frac{\partial}{\partial n}\left(\frac{1}{R}\right) - \frac{\partial \phi}{\partial n}\frac{1}{R} \right\} dS \tag{A.1}$$

where

$$R = \sqrt{(x-\xi)^2 + (y-\eta)^2 + (z-\zeta)^2} \tag{A.2}$$

and

$$\beta = \begin{cases} 4\pi, \text{ in } V \\ 2\pi, \text{ on } \partial V \\ 0, \text{ in } V^c \end{cases} \tag{A.3}$$

We may express the integral in terms of cylindrical coordinates as

$$\beta\phi = \iint_S \left\{ \phi \frac{\partial}{\partial n}\left(\frac{1}{R}\right) - \frac{\partial \phi}{\partial n}\frac{1}{R} \right\} ds\, d\varphi \tag{A.4}$$

where s denotes arclength and now

$$R = \sqrt{r^2 + \rho(s)^2 - 2\, r\, \rho(s) \cos(\theta - \varphi)} \tag{A.5}$$

If one now assumes the function ϕ has no dependence on φ, then the integration may be performed over φ to arrive at

$$\beta\phi = \int_C \left\{ \phi \frac{\partial G}{\partial n} - \frac{\partial \phi}{\partial n} G \right\} ds \tag{A.6}$$

where

$$G = \int_0^{2\pi} \frac{d\varphi}{\sqrt{r^2 + \rho^2 - 2r\rho\cos(\varphi)}} \tag{A.7}$$

or (see Gradshteyn and Ryzhik, 1965)

$$G = \frac{4\eta\, K(k)}{\sqrt{(y+\eta)^2 + (x-\xi)^2}} \tag{A.8}$$

where

$$k^2 = \frac{4y\eta}{(x-\xi)^2 + (y+\eta)^2} \tag{A.9}$$

Similarly,

$$\frac{\partial G}{\partial n} = n_\xi \frac{\partial G}{\partial \xi} + n_\eta \frac{\partial G}{\partial \eta} \tag{A.10}$$

where

$$\frac{\partial G}{\partial \xi} = \frac{-4\eta\,(x-\xi)\,E(k)}{(A-B)\sqrt{A+B}} \tag{A.11}$$

and

$$\frac{\partial G}{\partial \eta} = \frac{-2}{(A-B)\sqrt{A+B}} \left\{ \left[(x-\xi)^2 + (y-\eta)^2 \right] K(k) - \left[(x-\xi)^2 + y^2 - \eta^2 \right] E(k) \right\} \tag{A.12}$$

where

$$\begin{aligned} A &= (x-\xi)^2 + y^2 + \eta^2 \\ B &= 2\eta y \end{aligned} \tag{A.13}$$

In the above expression K and E represent complete elliptic integrals of the first and second kind respectively (see e.g. Abramowitz and Stegun, 1972). More details and extensions of this derivation may be found in Uhlman (1998).